DOI: 10.1002/ejic.200601194

Synthesis, Structure and Magnetic Properties of a Novel Hexanuclear Copper Methylsiloxane Complex

Larissa Zherlitsyna,[a] Norbert Auner,*[a] Michael Bolte,[a] Yulia Pozdniakova,[b] Olga Shchegolikhina,[b] Konstantin Lyssenko,[b] Vladimir Pashchenko,*[c] Bernd Wolf,[c] Michael Lang,[c] Florian Schütz,[d,e] Marcus Kollar,[f] Francesca Sauli,[d] and Peter Kopietz[d]

Keywords: Copper / Cluster compounds / Sandwich complexes / Magnetic properties

A new hexanuclear copper(II) sandwich complex based on two 12-membered macrocyclic methylsiloxanolate ligands, $[Cu_6\{(MeSiO_2)_6\}_2]\cdot 6DMF$, was synthesized and characterized by single-crystal X-ray diffraction analysis and magnetic measurements. The cluster compound crystallizes in the monoclinic system, space group $P2_1/n$ (No. 14), with a = 13.3728(5) Å, b = 15.4281(7) Å, c = 17.4335(7) Å, β = 98.932(3)° and Z = 2. The unit cell contains two identical molecular clusters, each consisting of six interacting Cu^{2+} (S = ½) ions. Within the cluster the six oxygen-bridged Cu^{2+} ions are arranged in an almost regular hexagon. An analysis of the high-temperature part of the magnetic susceptibility reveals that the complex has a strong average ferromagnetic Cu–Cu exchange interaction of $|J_{av}/k_B|$ = (50.4 ± 1) K with a high-spin S = 3 ground state. A satisfactory fit for the magnetic susceptibility and the magnetization in the whole accessible temperature range is obtained from a Heisenberg model with nonuniform exchange couplings within a ring, corresponding to a system of two weakly coupled trimers with a ferromagnetic intratrimer exchange coupling of $|J/k_B|$ = 72.5 K and a ferromagnetic intertrimer exchange coupling of $|J'/k_B|$ = 7 K.

Introduction

Because of their unusual physical properties, large metal clusters have attracted much attention during the past two decades.[1,2] In particular, the ability of transition-metal clusters to form single-molecule magnets has stimulated the research community to synthesize new compounds with various exchange interactions between the magnetic ions within a cluster.[1–3] In addition, different spin configurations within a cluster, together with possible magnetic exchange between neighbouring clusters, are of interest in molecular and low-dimensional magnetism because these systems may play an important role in future applications.

From a widespread series of molecular polymetallaorganosiloxane complexes, we have concentrated our interest on the family $[M_N\{(RSiO_2)_N\}_2]\cdot N$(Ligand) (where M = Ni, Mn, Co, Cu,…; N = 6, 8, 10,…; R = Et, Ph, Me,…; Ligand = EtOH, DMF,…), having a sandwich-like molecular structure. In the past decades, some representatives of this family have been obtained and their molecular structures have been established by single-crystal X-ray analysis.[4–8] These clusters are composed of two 2N-membered (N Si + N O) cycloorganosiloxanolate fragments linked together through N metal atoms. These polymetallaorganosiloxane complexes offer the potential to study the magnetic properties of molecular quantum rings experimentally. It should be noted that in a subfamily of copper-containing organosiloxanes with N = 6, only three representatives of hexanuclear copper(II) siloxanes with phenyl substituents at silicon atoms, $[Cu_6\{(PhSiO_2)_6\}_2]\cdot 6EtOH$, $\{[Cu_6\{(PhSiO_2)_6\}_2]\cdot 6DMF\}\cdot 4DMF$ and $\{[Cu_6\{(PhSiO_2)_6\}_2]\cdot 5BuOH\}\cdot 3^nBuOH$, have been described in the literature.[4,6,8] For the previously reported ring-shaped molecular complex $[Cu_6\{(PhSiO_2)_6\}_2]\cdot 6EtOH$,[9] it was demonstrated that the six copper ions within the ring are ferromagnetically coupled (J/k_B = –60 K) with a total spin S_{tot} = 3 ground state. The complex $\{[Cu_6\{(PhSiO_2)_6\}_2]\cdot 5BuOH\}\cdot 3^nBuOH$ also has a high-spin S_{tot} = 3 ground state, but its magnetic data indicate a strong nonequivalence of exchange pathways

[a] Institut für Anorganische Chemie, J. W. Goethe-Universität Frankfurt, FOR 412,
60439 Frankfurt (M), Germany
Fax: +49-69-798-29188
E-mail: auner@chemie.uni-frankfurt.de
[b] A. N. Nesmeyanov Institute of Organoelement Compounds of RAS (INEOS),
28 Vavilov Str., 117813 Moscow, Russia
[c] Physikalisches Institut, J. W. Goethe-Universität Frankfurt, FOR 412,
60438 Frankfurt (M), Germany
Fax: +49-69-798-47250
E-mail: pashchenko@physik.uni-frankfurt.de
[d] Institut für Theoretische Physik, J. W. Goethe-Universität Frankfurt, FOR 412,
60438 Frankfurt (M), Germany
[e] Department of Physics, Brown University,
Providence, RI 02912, USA
[f] Theoretische Physik III, Universität Augsburg,
86135 Augsburg, Germany
Supporting information for this article is available on the WWW under http://www.eurjic.org or from the author.

within the ring (J_1/k_B = –89.2 K, J_2/k_B = –15.3 K).[8] For more detailed investigations on the mechanisms leading to the formation of a high-spin ground state and the influence of various substituents and/or ligands of the molecule on the magnetic behaviour of the quantum ring, we have attempted to expand the existing class of copper-containing molecular magnets by the synthesis of new isostructural molecular complexes.

Here we report on the synthesis, structure and magnetic properties of a novel sandwich-like hexacopper hexamethylcyclohexasiloxane complex, $[Cu_6\{(MeSiO_2)_6\}_2]\cdot 6DMF$. In contrast to the phenyl analogues previously reported,[4,6,8] the present complex has methyl groups as substituents at the silicon atoms. Preliminary results of this work have been published in ref.[10], in which the high-temperature susceptibility of this complex has been analyzed and an initial comparative investigation of the structural and magnetic properties has been carried out.

Results and Discussion

The synthesis of sandwich-like polyhedral metallaorganosiloxanes containing transition metals is commonly based on an exchange reaction of alkali-metal organosiloxanolates[11] with transition-metal chlorides in alcohol-containing media.[4–6,12,13]

Similarly, the novel copper methylsiloxane $[Cu_6\{(MeSiO_2)_6\}_2]\cdot 6DMF$ (**E**) has been obtained in a two-step reaction (Scheme 1). The first step involves an alkaline hydrolysis of methyltriethoxysilane $MeSi(OEt)_3$ (Si/KOH ratio of 1:1) in a toluene/methanol mixture generating in situ a potassium methylsiloxanolate intermediate **A**. A spontaneous association of potassium methylsiloxanolate intermediates **A** leads to the formation of aggregates **B**, in which an ionic network containing alcohol and water molecules is surrounded by organosilicon species with functional groups. In a second step, the addition of a methanolic solution of $CuCl_2$ (Cu/K ratio of 1:2) initiates an irreversible exchange reaction that substitutes the potassium ions with copper ions. Consequently, potassium chloride precipitates from the reaction. Thus, aggregates **B**, originally containing only alkali metals, are reorganized into new aggregates **C**, now possessing only copper atoms. Finally, condensation of EtO– and OH– functional groups at silicon results in the formation of the cyclic siloxane fragments.

After filtration of precipitated KCl, complete evaporation of the solvent from aggregates **C** gives a greenish-blue product **D** with a yield up to 82.5%. A powder X-ray diffraction analysis (XRD) of the obtained product **D** proved that the product was in the crystalline state. However, the crystals were too small for single-crystal X-ray analysis.

To identify product **D**, we used a well-known approach applied in organosilicon chemistry, preparing the trimethylsilyl-substituted derivative of the functional system. This general route was optimized for the treatment of metallaorganosiloxanes.[13] According to Scheme 2, the cyclic siloxane fragments of the starting metallaorganosiloxanes were isolated as a trimethylsiloxy derivative with retention of the

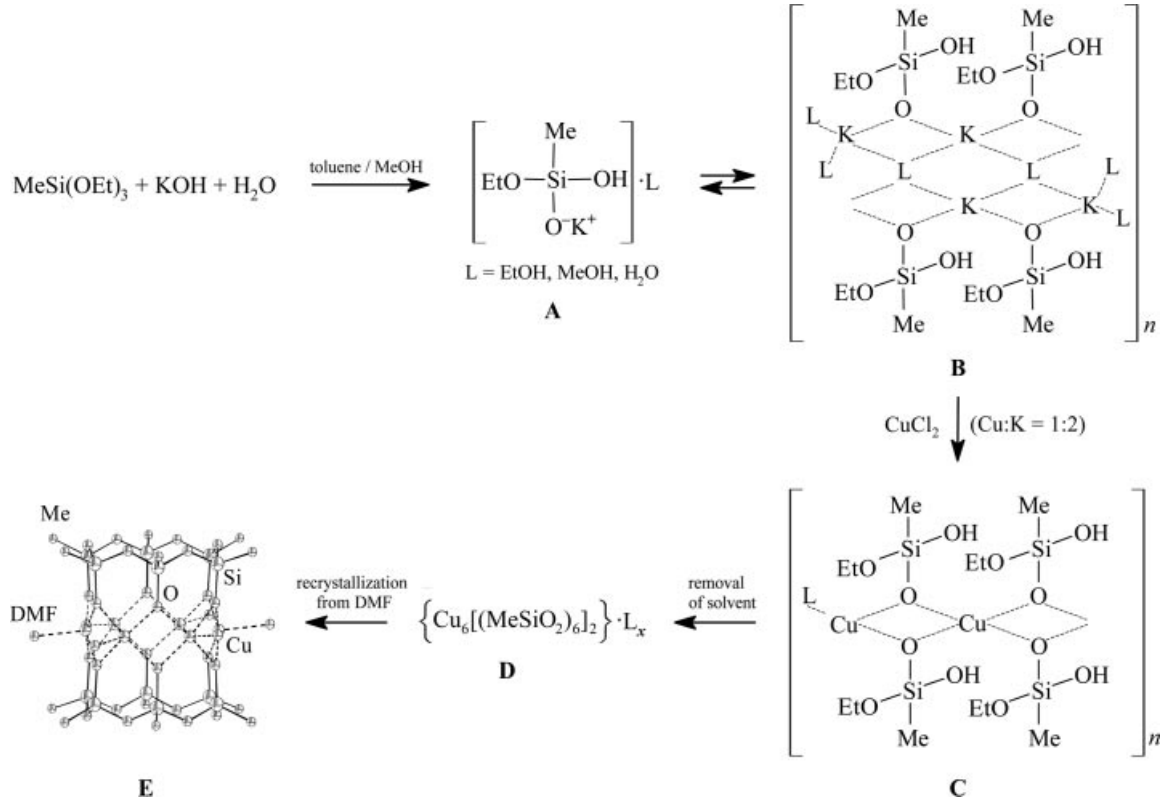

Scheme 1.

size and configuration of the rings. Consequently, the correspondence of crystalline **D** to the formula $[Cu_6\{(MeSiO_2)_6\}_2]\cdot L_x$ was confirmed by its trapping reaction with Me_3SiCl and subsequent NMR spectroscopy investigations on the resulting product.

$$\left\{Cu_6[(MeSiO_2)_6]_2\right\}\cdot L_x + Me_3SiCl \xrightarrow[-\,CuCl_2]{\text{py, hexane}} \left[MeSi(O)(OSiMe_3)\right]_6$$

Scheme 2.

The ^1H NMR spectrum of $[MeSi(O)(OSiMe_3)]_6$ exhibits two nonequivalent signals for the methyl groups: one singlet at 0.11 ([–$SiMe_3$]) and one singlet at δ = 0.03 ppm ([MeSi–]), with an integrated intensity ratio of 3:1.

The ^{29}Si NMR spectrum of $[MeSi(O)(OSiMe_3)]_6$ shows two signals: one singlet at δ = 8.50 ppm corresponds to the [–$OSiMe_3$] groups and the second one at –68.18 ppm ([Me-SiO_3–]) to the Si atoms in the hexamethylcyclohexasiloxanolate ring $[MeSi(O)O^-]_6$.

As the dried product **D** is insoluble in methanol, toluene or ethanol, DMF was used as a solvent for recrystallization, giving greenish-blue crystals **E** after a few months. X-ray analysis on suitable single crystals proved the product to be $[Cu_6\{(MeSiO_2)_6\}_2]\cdot 6DMF$. It should be noted that the crystals are very unstable in air because the desolvating occurs within a short time period, thereby reducing the properties of the crystal transparency.

Crystal Structure of $[Cu_6\{(MeSiO_2)_6\}_2]\cdot 6DMF$

In accordance with the single-crystal X-ray analysis, the complex $[Cu_6\{(MeSiO_2)_6\}_2]\cdot 6DMF$ crystallizes in the monoclinic system, space group $P2_1/n$ (no. 14) with a = 13.3683(14) Å, b = 15.388(2) Å, c = 17.4383(14) Å, β = 98.88(7)° and Z = 2.

The complex $[Cu_6\{(MeSiO_2)_6\}_2]\cdot 6DMF$ exhibits a ring-shaped sandwich-like structure (Figure 1). The molecule consists of two hexamethylcyclohexasiloxanolate ligands, $[(MeSiO_2)_6]^{6-}$, sandwiched by six Cu^{2+} ions. Within the ring, the adjacent Cu^{2+} ions are linked by pairs of siloxanolate oxygen atoms, which provide the main magnetic exchange path for the copper S = 1/2 spins. The overall molecular building topology is analogous to that of the hexacopper(II) cyclohexaphenylsiloxanolates $[Cu_6\{(PhSiO_2)_6\}_2]\cdot 6EtOH$,[4] $\{[Cu_6\{(PhSiO_2)_6\}_2]\cdot 6DMF\}\cdot 4DMF$[6] and $\{[Cu_6\{(PhSiO_2)_6\}_2]\cdot 5BuOH\}\cdot 3^nBuOH$[8] described earlier.

It is important to note that the molecular structure of $[Cu_6\{(MeSiO_2)_6\}_2]\cdot 6DMF$ is centrosymmetric, with a crystallographic inversion centre at the midpoint of the molecule. The molecules of the complexes $\{[Cu_6\{(PhSiO_2)_6\}_2]\cdot 6DMF\}\cdot 4DMF$ and $\{[Cu_6\{(PhSiO_2)_6\}_2]\cdot 5BuOH\}\cdot 3^nBuOH$ also contain a crystallographic centre of inversion, while the complex $[Cu_6\{(PhSiO_2)_6\}_2]\cdot 6EtOH$ shows a higher local symmetry of the molecules (trigonal symmetry C_3), giving only two symmetry-independent positions for copper atoms.

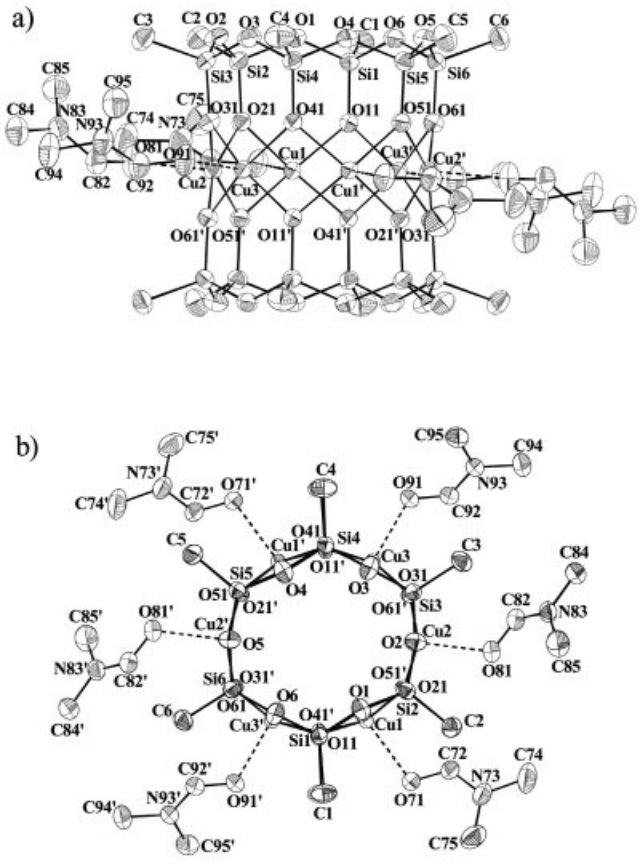

Figure 1. Side view (a) and top view (b) of the molecular structure of the complex $[Cu_6\{(MeSiO_2)_6\}_2]\cdot 6DMF$ with the atomic labelling. The hydrogen atoms have been omitted for clarity. The dashed bonds indicate the apical coordination of the copper atoms. Displacement ellipsoids are drawn at the 50% probability level.

The hexamethylcyclohexasiloxanolate ligands have an *all-cis* configuration; the olate groups are directed towards the plane of the Cu atoms. The two 12-membered siloxanolate $(Si–O)_6$ rings are coaxial and parallel to each other. The Si–O(Si) bond lengths vary in the range of 1.624–1.636 Å and the Si–O–Si angles in the range of 133.98–136.64°, which are usual for this class of compounds.[4,5,7] The standard deviations of the Si and O atoms from the mean planes do not exceed 0.0004 Å and 0.0012 Å, respectively. The Si–O(Cu) bond lengths are significantly shorter (1.609–1.613, av. 1.611 Å) than the corresponding Si–O(Si) bond lengths in the hexasiloxane macrocycle. The Si–O–Si sections of the siloxanolate ring are nearly perpendicular to the mean plane of the Si atoms (dihedral angles 74.3–89.3°). The methyl group, attached to each of the 2×6 Si atoms, points away from the molecule.

A metal group of the six Cu^{II} atoms is arranged as an almost flat (standard deviation from the mean plane is 0.0002 Å) hexagon. In contrast to the complex $[Cu_6\{(PhSiO_2)_6\}_2]\cdot 6EtOH$,[4] which has a high (trigonal) crystal symmetry, the hexagon in the complex $[Cu_6\{(MeSiO_2)_6\}_2]\cdot 6DMF$ is slightly distorted. However, this distortion of the hexahedron is significantly smaller compared with the observed one in the complex

{[Cu_6{$(PhSiO_2)_6$}$_2$]·6DMF}·4DMF.[6] In all cases the Cu, Si, O skeleton approaches 6/*mmm* symmetry. In the complex [Cu_6{$(MeSiO_2)_6$}$_2$]·6DMF the nonbounded Cu–Cu distances are 2.816, 2.841 and 2.861 Å (av. 2.839 Å) and the distance between opposite copper atoms varies between 5.495(7) and 5.820(6) Å (av. 5.677 Å).

The coordination surrounding of the copper atoms in the complex [Cu_6{$(MeSiO_2)_6$}$_2$]·6DMF is a slightly distorted oxygen square-pyramidal (SP) configuration. It should be noted that, similarly to the known sandwich-like complexes,[4,6,8] the copper–oxygen moiety is organized in the cyclic form by the oxygen atoms of the siloxanolate ligands and the SP configuration arises from the apical oxygen bonding with the solvent molecules. In the further discussion, the oxygen atoms of the siloxanolate ligands bound to the copper atoms will be indicated as equatorial, whereas the others, belonging to the DMF solvent, will be mentioned as apical or axial.

The equatorial Cu–O bonds in the complex vary in the range of 1.946–1.974 Å (av. 1.957 Å), which is close to the expected values for copper atoms with a square-pyramidal coordination environment. In the recently reported copper-containing siloxanolate complexes,[4,6,8] it was demonstrated that the average Cu–O bond lengths in the basal plane for SP (av. 1.96 Å) and in the case of square-planar configuration (av. 1.90 Å) are significantly different. The Cu–O–Cu angles at the bridging equatorial oxygen atoms, which mainly determine the magnetochemical behaviour of polynuclear clusters, vary in the range 91.26–94.59°, which is typical for other copper-containing sandwich-like organosiloxanes.[4,6,8] The average value of the Cu–O–Cu angle is about 93.02°.

All copper atoms are shifted from the mean planes of the slightly distorted basal squares of the equatorial oxygen atoms by 0.324 (for Cu1), 0.290 (Cu2) and 0.323 Å (Cu3) towards the external axially coordinated oxygen of DMF molecules. In the close analogues [Cu_6{$(PhSiO_2)_6$}$_2$]·6EtOH and {[Cu_6{$(PhSiO_2)_6$}$_2$]·6DMF}·4DMF, the shifts are 0.285(Cu1)–0.290(Cu2) and 0.345(Cu1)–0.288(Cu2)–0.349(Cu3) Å, respectively.

The six apical positions of all copper polyhedra in the complex $Cu_6[(MeSiO_2)_6]_2$·6DMF are occupied by the DMF oxygen atoms and the corresponding Cu–O bonds are always significantly longer than the equatorial ones. The apical Cu–O bonds vary in the range of 2.229(3)–2.322(6) Å (av. 2.273 Å).

Selected bond lengths and bond angles are summarized in Table 1.

Interestingly, in contrast to the complex {[Cu_6{$(PhSiO_2)_6$}$_2$]·6DMF}·4DMF described earlier,[6] which was also recrystallized from DMF, the crystal structure of [Cu_6{$(MeSiO_2)_6$}$_2$]·6DMF does not contain any additional solvate molecules within the intermolecular space.

It should be noted that the central cavity of the molecule contains a relatively large empty inner channel, suitable for small molecules or ions to enter the interior of the complex. The estimated diameter of the free cross-section is about 2.5 Å. Despite the similarity in the overall molecular building topology, the presence of an additional small anion, occupying the central cavity, was observed only for non-copper-containing metallasiloxanes (with Ni, Co, Mn).[5,7]

Table 1. Selected bond lengths [Å] and angles [°] for [Cu_6{$(MeSiO_2)_6$}$_2$]·6DMF.

Bond lengths [Å]			
Cu1–O11	1.9457(10)	Si1–O1	1.6235(12)
Cu1–O41′[a]	1.9460(10)	Si1–O11	1.6095(11)
Cu1–O21	1.9606(10)	Si1–O6	1.6244(11)
Cu1–O51′	1.9611(10)	Si1–C1	1.8424(18)
Cu1–O71	2.3256(12)	Si2–O1	1.6315(12)
Cu2–O31	1.9485(11)	Si2–O21	1.6091(11)
Cu2–O21	1.9531(10)	Si2–O2	1.6282(13)
Cu2–O51′	1.9543(11)	Si2–C2	1.8523(16)
Cu2–O61′	1.9654(10)	Si3–O2	1.6328(12)
Cu2–O81	2.2625(13)	Si3–O31	1.6092(11)
Cu3–O11′	1.9481(10)	Si3–O3	1.6285(12)
Cu3–O31	1.9613(10)	Si3–C3	1.8411(18)
Cu3–O41	1.9664(10)	Si4–O3	1.6219(12)
Cu3–O61′	1.9739(10)	Si4–O41	1.6123(11)
Cu3–O91	2.2311(13)	Si4–O4	1.6258(13)
Cu1–Cu2	2.8412(3)	Si4–C4	1.8458(19)
Cu2–Cu3	2.8159(3)	Si5–O4	1.6285(12)
Cu1–Cu3′	2.8614(3)	Si5–O51	1.6110(12)
Bond angles [°]			
Cu1–O11–Cu3′	94.589(44)	Cu2–O61′–Cu3	91.258(45)
Cu1–O41′–Cu3′	93.998(45)	Cu2–O21–Cu1	93.098(47)
Cu2–O31–Cu3	92.141(45)	Cu2–O51′–Cu1	93.047(46)

[a] Symmetry transformations used to generate equivalent atoms: (′) $-x + 1, -y + 1, -z + 1$.

The crystal packing of the complex is shown in Figure 2. The structure consists of two nonequivalent layers of [Cu_6{$(MeSiO_2)_6$}$_2$]·6DMF molecules, which are parallel to the crystallographic (*ac*) plane. The local axis of the molecules for the neighbouring layers are turned from the normal to the (*ac*) plane and make up an angle of 25.76° with the crystallographic *b* axis.

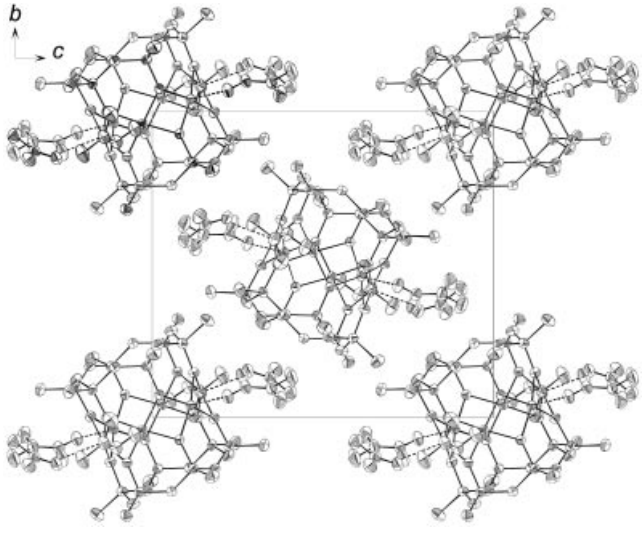

Figure 2. Crystal packing of the complex [Cu_6{$(MeSiO_2)_6$}$_2$]·6DMF, viewed along the [100] direction. The hydrogen atoms have been omitted for clarity.

Magnetic Properties of $[Cu_6\{(MeSiO_2)_6\}_2]$·6DMF

Magnetic susceptibility and magnetization measurements were performed on polycrystalline samples of $[Cu_6\{(MeSiO_2)_6\}_2]$·6DMF. The data were corrected for the contribution of the sample holder and for the diamagnetic core contribution. Notably, the temperature-independent contribution of $\chi_0 = -3.29 \times 10^{-3}$ cm^3/mol, determined by analyzing the high-temperature magnetic behaviour, is in reasonable agreement with the sum of the sample holder contribution of $\chi_{sholder} \approx -1.9 \times 10^{-3}$ cm^3/mol and the core contribution of $\chi_{core} = -1.37 \times 10^{-3}$ cm^3/mol calculated by using tabulated values for Pascal's constants.[14]

Figure 3 shows the molar magnetic susceptibility $\chi(T) = M(T)/B$ of complex $[Cu_6\{(MeSiO_2)_6\}_2]$·6DMF, where M denotes the magnetic moment of the sample per mole. The data were found to be reversible upon cooling and heating, with no indications for hysteretic behaviour. Moreover, no sign of long-range magnetic ordering was observed in the temperature range under investigation. From isothermal magnetization measurements in dc fields from 0 to 5 T at varying temperatures (see Figure 6), we have also extracted the data for the differential magnetic susceptibility $[dM(T)/dB]_{B\to 0}$, which are indicated as the solid star symbols in Figure 3. The collapse of the susceptibility data onto a single curve shows that no significant field dependence occurs over the whole temperature (2–350 K) and field (0.01–0.2 T) range under investigation.

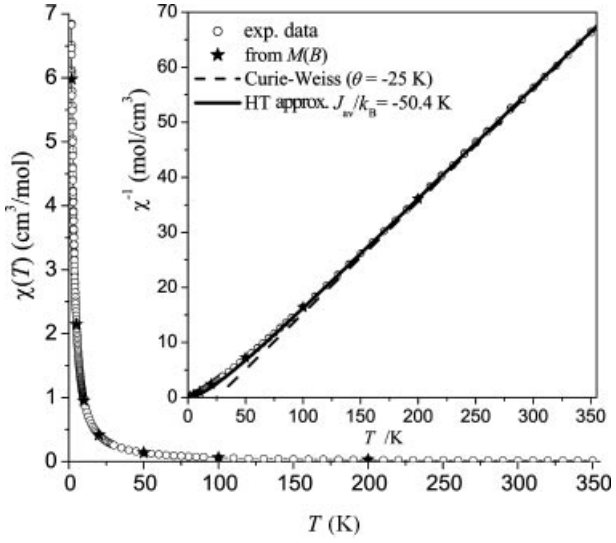

Figure 3. Temperature dependence of the magnetic susceptibility of complex $[Cu_6\{(MeSiO_2)_6\}_2]$·6DMF for temperatures 2–350 K. The data have been taken at magnetic fields of 0.01–0.2 T. Star symbols denote the susceptibility data extracted from isothermal magnetization measurements. The inset shows the inverse magnetic susceptibility. The solid line corresponds to the best fit using the high-temperature approximation Equation (2) with the parameter $J_{av}/k_B = (-50.4 \pm 1)$ K in the range 100–350 K. The dashed line corresponds to the calculated curve by using a simple Curie–Weiss law $\chi(T) = C/(T + \theta)$ for the six-site ring ($S = 1/2$; $g = 2.10$) with $\theta = -25$ K.

The analysis of the magnetic properties of the complex $[Cu_6\{(MeSiO_2)_6\}_2]$·6DMF was performed in the following three steps. First, in the high-temperature range, we used a Curie–Weiss law to obtain preliminary information on the sign and average magnitude of the exchange interactions between the six Cu^{2+} ($S = 1/2$) ions inside the molecule. Next, in analogy to what has been done for other ring-shaped complexes,[8,9] we attempted to analyze the obtained experimental data within the framework of a model with uniform exchange couplings between nearest-neighbour spins within the ring. We found that this uniform exchange coupling model, even with the possible extensions such as significant intermolecular interactions, weakly anisotropic intramolecular exchange interactions or next-nearest neighbour exchange couplings, is not capable of satisfactorily reproducing the low-temperature part of the magnetic behaviour of this compound. In a third step, taking into account the structural symmetry properties of the molecule, we thus considered the most general Heisenberg model for the six-site ring with three a priori nonequivalent exchange couplings. This nonuniform nearest-neighbour exchange model, which has a parameter set corresponding to a pair of weakly coupled trimers with a strong ferromagnetic intratrimer coupling and a weak ferromagnetic intertrimer coupling, yields a satisfactory agreement with the observed experimental data.

Magnetic Susceptibility at High Temperatures

In a first attempt at setting up a simple model capable of describing the main features of the magnetic susceptibility of the complex $[Cu_6\{(MeSiO_2)_6\}_2]$·6DMF at high temperatures, the magnetic behaviour can be assigned to a Curie–Weiss-like temperature dependence $\chi(T) = C/(T + \theta)$ with a Curie constant C and a Weiss temperature θ. In the temperature range 100–350 K, the best fit yields $C = 5.041$ cm^3 K/mol and $\theta = -17.7$ K. The obtained Curie constant is consistent with the presence of six Cu^{2+} ions per molecule (two molecules per unit cell) yielding a spin-only value of $C_{theory} = 4.914$ cm^3 K/mol. The latter number is based on an average spectroscopic g-value of 2.10 ± 0.02, as determined by our high-temperature ESR measurements operated at X- and Q-band frequencies. It should be noted that all known ring-shaped copper complexes[4,6,8] have a similar square-pyramidal oxygen configuration of the nearest environment of the copper ions, therefore a quite close value of the average spectroscopic g-factor for the local magnetic centre is expected. For the recently reported phenyl analogues,[8,9] it was found that the average g-values of the Cu^{2+} ions are in the range 2.11–2.12. The negative Weiss constant θ indicates a dominant ferromagnetic spin–spin interaction. It should be noted that a simple Curie–Weiss law implies a temperature-independent effective moment of the magnetic centres, which results in a strictly linear behaviour of the inverse magnetic susceptibility. As can be seen in the inset of Figure 3, the inverse magnetic susceptibility of the complex exhibits a weak nonlinearity over the entire high-temperature region and an appropriate microscopic magnetic model would be desirable.

In search of a minimal microscopic model, we first assume isotropic Heisenberg exchange between nearest-neighbour spins in the ring, ignoring possible complications such as next-nearest neighbour couplings or anisotropic exchange interactions. Because of the inversion centre of the molecule (see Figure 1, b), bonds on opposite sites of the ring that are mapped onto each other by the symmetry transformation are equal and the most general Heisenberg model is given by Equation (1)

$$H = J_1(\mathbf{S}_1 \cdot \mathbf{S}_2 + \mathbf{S}_4 \cdot \mathbf{S}_5) + J_2(\mathbf{S}_2 \cdot \mathbf{S}_3 + \mathbf{S}_5 \cdot \mathbf{S}_6) + J_3(\mathbf{S}_3 \cdot \mathbf{S}_4 + \mathbf{S}_6 \cdot \mathbf{S}_1) - g\mu_B B \sum_{i=1}^{6} S_i^z \quad (1)$$

with three a priori nonequivalent exchange couplings, J_1, J_2 and J_3, which, from the molecular structure, might be expected to be close in magnitude. However, this expectation turns out not to be justified, as we will discuss in the next section. In Equation (1), $\mathbf{S}_i$ are spin-1/2 operators located at the Cu sites of the ring, μ_B is the Bohr magneton and g is an average spectroscopic g-value of Cu^{2+} ions.

A first estimate of the strength of the exchange couplings can be obtained from a high-temperature expansion of the magnetic susceptibility. The first terms are given by Equation (2)

$$\chi|_{h=0} = \frac{N\mu_B^2 g^2}{k_B} \frac{3}{2T}\left\{1 - \frac{J_{av}}{2k_B T} + O\left(\frac{Ji^2}{T^2}\right)\right\} \quad (2)$$

where $J_{av} = (J_1 + J_2 + J_3)/3$ is the average exchange interaction within the ring.[10,15] In Equations (2)–(4), N is the number of spins and k_B is the Boltzmann constant. For uniform exchange couplings $J_1 = J_2 = J_3$, we have compared this high-temperature approximation with results of a complete numerical diagonalization for spin $S = 1/2$ rings with $N = 6$ and concluded that this is in satisfactory agreement with the exact solution for temperatures above $3/2 \cdot J_{av}$.

In the inset of Figure 3 the solid line shows the best fit of the high-temperature expansion Equation (2) to the experimental data with the parameter $J_{av}/k_B = (-50.4 \pm 1)$ K. It should be noted that at high temperatures, the leading terms in the high-temperature expansion agree with the Curie–Weiss law, where, by expanding the latter in powers of $1/T$, one obtains $J_{av}/k_B = 2\theta$.

Magnetic Behaviour at Low Temperatures

Before starting the discussion of the low-temperature part, a few interesting peculiarities of the low-temperature magnetic behaviour of the present complex observed in the experiment should be underlined. At $T = 2$ K, the product $\chi(T) \cdot T$ reaches a value of approximately 12 $cm^3/mol\,K$, which is close to what would be expected for two effective spins $S = 3$ per unit cell, but with an effective spectroscopic g-value $g = 2.00$, yielding $\chi \cdot T = 12.004\ cm^3/mol\,K$. Of course, this can be due to the fact that at the given temperature ($T = 2\ K \approx \frac{1}{25}|J_{av}/k_B|$) the system has not yet frozen into the state with full ferromagnetic alignment and a tendency toward the higher value of $2 \times (S = 3;\ g = 2.10) \rightarrow 13.234\ cm^3/mol\,K$ is observable (see the inset of Figure 4). Note that Figure 4 shows the normalized square of the effective moment $\chi \cdot T/(N\mu_B^2 g^2/k_B)$ of the complex $[Cu_6\{(MeSiO_2)_6\}_2] \cdot 6DMF$ (where we set $g = 2.10$) as a function of normalized temperature T/J_{av}. Additionally, the experimentally observed magnetization $M(B)$ of the complex at $T = 2$ K can be nicely reproduced by a Brillouin function for an effective spin $S = 3$, again with $g = 2.00$ (see the dashed line in Figure 6). The reason for this "high symmetry" isotropic behaviour of the effective g-tensor of the magnetic molecular cluster is not clear.

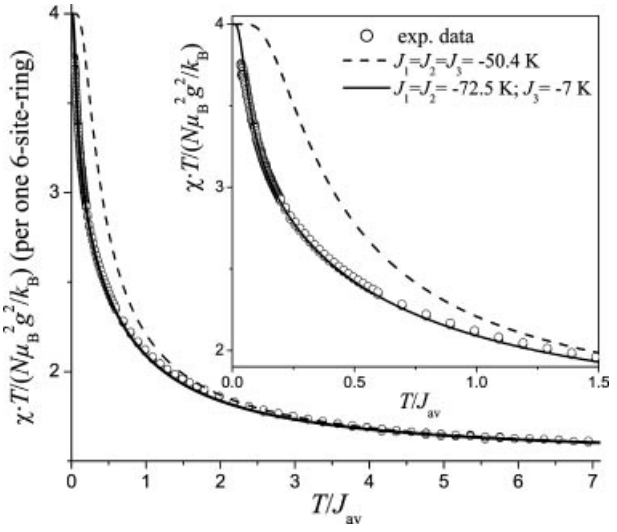

Figure 4. The product $\chi \cdot T/(N\mu_B^2 g^2/k_B)$ as a function of normalized temperature T/J_{av}. The inset shows the low-temperature behaviour on expanded scales. The dashed line indicates the theoretical result of a complete numerical diagonalization for uniform ferromagnetic exchange couplings within the ring. The solid line corresponds to the best fit for a nonuniform exchange coupling model.

In the case of uniform ferromagnetic couplings $J_1 = J_2 = J_3$ within the ring (as well as in the presence of weak anisotropy of these interactions), the parameter $J_{av}/k_B = -50.4$ K strictly determines the initial structure of the energy spectrum and, therefore, the quantitative characteristics of the crossover (the temperature evolution of the effective magnetic moment of the molecular cluster) from a low-temperature plateau of width $\sim\Delta/2 = \frac{1}{4}|J_{av}/k_B| = 12.6$ K to the $1/T$ behaviour at high temperatures discussed in the previous section. Here, $\Delta = |J| \cdot [1 - \cos(2\pi/N)] = |J|/2$ is the finite-size gap of spin-wave excitations above the high-spin ferromagnetic ground state corresponding to the splitting between the lowest two levels. The lowest levels of the resulting energy-level scheme for a model with uniform exchange couplings with $J_{av}/k_B = -50.4$ K are sketched in Figure 5 (left part). In Figure 4, the numerical result for the product $\chi \cdot T/(N\mu_B^2 g^2/k_B)$ for the uniform-exchange model with $J_{av}/k_B = -50.4$ K is shown as a black dashed line. A

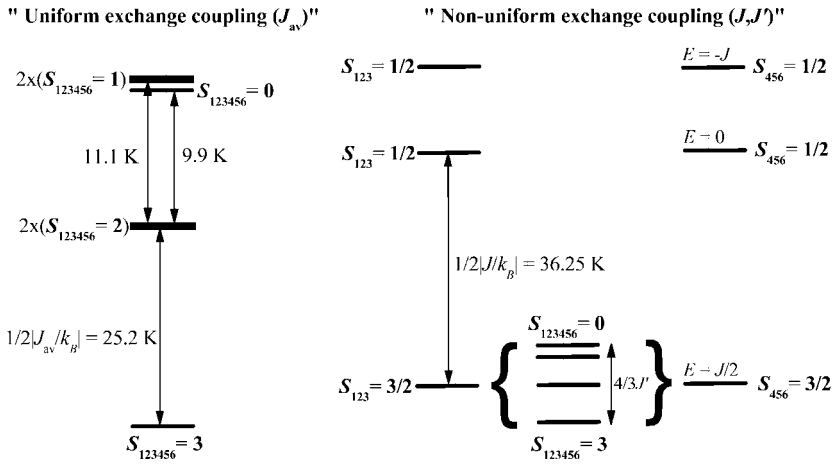

Figure 5. Energy-level schemes for a uniform ferromagnetically coupled ring (left part) with J_{av} and for two weakly coupled trimers (right part) with a strong ferromagnetic intratrimer coupling J and a weak ferromagnetic intertrimer coupling J'. Only the splitting of the high-spin ground state of the complex due to the coupling J' is considered, as the splitting of excited states is not relevant for the thermodynamic quantities in the temperature and field range considered here.

closer look at the experimental data in Figure 4 reveals that $\chi \cdot T/(N\mu_B{}^2g^2/k_B)$ does not show a low-temperature plateau in the accessible temperature range. This indicates that the ground state of the magnetic cluster might be composite, and the presence of other energy levels at a distance of a few Kelvin from the ground $S_{123456} = 3$ multiplet is possible. Furthermore, Figure 4 reveals that significant deviations of the experimental data from the results for the uniform-exchange model with $J_{av}/k_B = -50.4$ K become visible at temperatures below approximately 100 K. A comparison to the total width of the spectrum of $|E_{FM} - E_{AFM}| = 8.6 \times 50.4/2 \approx 217$ K for this case already hints at the fact that to account for these deviations a significant adaptation of the model is required.

In order to fix further the parameters of the microscopic model, we analyzed the low-temperature behaviour of the magnetic susceptibility more carefully. To this end, the Hamiltonian in Equation (1) can easily be diagonalized numerically, as the dimension of the largest subspace to be considered is only 20 using the conservation of the z component of the total spin. For uniform exchange couplings $J_1 = J_2 = J_3$, even analytic results can be obtained exploiting translational invariance.[16] For convenience, we will only use numerical results here, as well as a perturbative treatment for $J_1 = J_2 \equiv J$ and $J_3 \equiv J'$, $|J'| << |J|$. In Figure 4 the presentation of the product $\chi \cdot T/(N\mu_B{}^2g^2/k_B)$ as a function of normalized temperature T/J_{av} has been chosen in order to simplify the comparison of the data with various theoretical predictions. Note also that the set of exchange coupling parameters $\{J_1, J_2, J_3\}$, extracted for a particular model, always have to be in agreement with the average value $J_{av}/k_B = -50.4$ K obtained from the high-temperature fit in the previous section.

The absence of a sizeable finite-size gap above the high-spin ferromagnetic ground state might be attributed to intermolecular interactions, either of dipolar or exchange type. However, rather large intermolecular distances and the absence of an apparent exchange path between neighbouring molecules lead us to search for intramolecular mechanisms to explain the low-temperature behaviour. As candidates, we have envisioned anisotropic intramolecular exchange and next-nearest neighbour exchange, as well as a nonuniform exchange.

Our low-temperature ESR measurements show a zero-field splitting in the order of 1 K, so that it seems natural to analyze the influence of anisotropies on the low-temperature behaviour of the susceptibility. Microscopically, such anisotropies can arise from anisotropic exchange interactions as well as intramolecular dipolar interactions. In the high-spin low-energy subspace they lead to an effective single-ion anisotropy term of the form $H = D(S^z_{tot})^2$, where $\mathbf{S}_{tot} = \mathbf{S}_1 + \ldots + \mathbf{S}_6$ and D can in principle be obtained as an average over the microscopic anisotropic exchange parameters. Yet, a quantitative analysis of such anisotropy terms reveals that the angular average of the susceptibility is only changed below a temperature scale in the order of D. Furthermore, $\chi \cdot T$ is reduced for $T \rightarrow 0$ and shows a maximum at a temperature $\sim D$. This behaviour is clearly not observed in the experiment and we conclude that the anisotropies seen in ESR measurements are too small to be relevant to thermodynamic quantities in the temperature range under consideration.

From a numerical treatment of next-nearest-neighbour exchange we find a slightly better fit to the experimental data than with just the nearest-neighbour exchange. Yet, the agreement is not satisfactory, as the functional form with a very steep decrease of $\chi \cdot T$ at low temperatures does not correspond to the experimentally observed curve.

To analyze nonuniform exchange, we consider $J_1 = J_2 = J$ and $J_3 = J'$, which might correspond, for example, to the following exchange links between the Cu1–Cu2, Cu2–Cu3 and Cu3–Cu1′ atoms, respectively. It turns out that for $|J'| << |J|$ a good fit of the experimental data can indeed be achieved. The model then reduces to two weakly coupled

trimers with a strong ferromagnetic intratrimer coupling J and a weak ferromagnetic intertrimer coupling J'. The solid line in Figure 4 shows the best fit of the effective magnetic moment with nonuniform exchange couplings, yielding J/k_B = –72.5 K and J'/k_B = –7 K. For these parameters, a perturbative treatment of the intertrimer coupling is possible. The resulting level scheme is sketched in Figure 5 (right part). The energy spectrum of an isolated ferromagnetic trimer consists of a quartet ground state separated from two excited doublets by an energy gap $|J/2|$ and $|3J/2|$, respectively. The ground-state splitting $4/3|J'|$ of two ferromagnetic trimers within the molecule is due to ferromagnetic intertrimer coupling. For the magnetization and the magnetic susceptibility, only the splitting of the high-spin ground state due to the intertrimer coupling J' is relevant and we can obtain analytic formulas, for example, the magnetic susceptibility is given by Equation (3)

$$\chi(T) = \frac{N\mu_B^2 g^2}{k_B}\,\frac{1}{2T}\,\frac{x^{-6}\left(1+x^2+2x^3\right)\left(1+x^2+10x^3\right)+\left(14y^9+5y^{-3}+y^{-11}-20\right)}{x^{-6}\left(1+x^2+2x^3\right)^2+\frac{1}{4}\left(7y^9+5y^{-3}+3y^{-11}+y^{-15}-16\right)} \tag{3}$$

where $x = \exp[-(J/2k_BT)]$ and $y = \exp[-(J'/18k_BT)]$. Equation (3) can be checked by comparison with numerical diagonalization for the full model. At least up to $|J'/J| \leq 0.1$, we obtain excellent agreement with the exact result. Note that for $J' \to 0$ Equation (3) results as expected in twice the susceptibility of an isolated ferromagnetic trimer. In contrast to the antiferromagnetically coupled trimer model described earlier,[3] the influence of J' on the magnetic susceptibility is rather strong and the deviations from the pure ferromagnetic trimer model become visible even at relatively high temperatures. This can be understood by noting that the saturation value of the product $\chi T|_{J' \to 0,\ T \to 0} = 5/2$ for two isolated trimers within a molecule is significantly reduced compared to $\chi T|_{J' \neq 0,\ T \to 0} = 4$ for the high-spin $S = 3$ ground state.

Magnetization Curves

The magnetization of the complex $[Cu_6\{(MeSiO_2)_6\}_2]\cdot 6DMF$ at various temperatures is shown in Figure 6 as a function of the applied magnetic field. In order to check the main result obtained from the analysis of the magnetic susceptibility, we have also calculated the isothermal magnetization curves for the above-discussed models of a uniform ferromagnetically coupled ring with J_{av}/k_B = –50.4 K and nonuniform exchange couplings with J/k_B = –72.5 K and J'/k_B = –7 K. The uniform-exchange model progressively departs from the experimental data below 100 K (calculated curves are not shown). On the other hand, a very good description, except for the data taken at the lowest temperature of 2 K, can be achieved by the model with nonuniform exchange couplings.

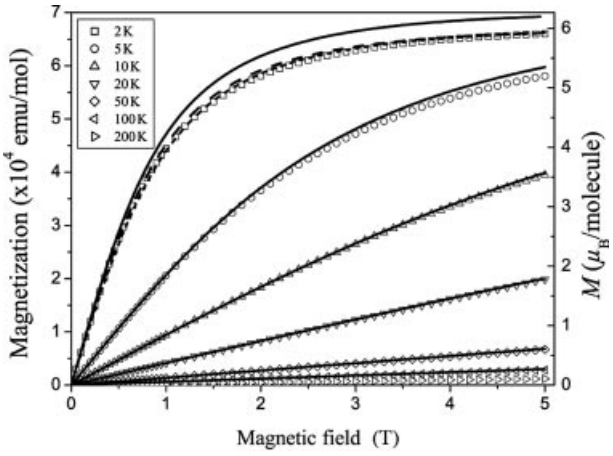

Figure 6. Isothermal magnetization measurements in dc fields from 0 to 5 T at varying temperatures as indicated in the figure. The right scale of the main panel is given in units of μ_B per molecule. The solid lines indicate the theoretical results for a nonuniform exchange coupling model with J/k_B = –72.5 K and J'/k_B = –7 K (g = 2.10). The dashed and short dashed lines correspond to the calculated magnetization curve (Brillouin function) at T = 2 K for isolated magnetic quasiparticles with S = 3 and g = 2.00 and for the above-mentioned nonuniform coupling model with g = 2.00, respectively.

For the model with nonuniform exchange couplings, we can obtain a perturbative analytic expression for the magnetization in Equation (4)

$$M(T,h) = N\mu_B g \cdot \frac{2x^{-6}\left(Z'_{½}+Z'_{½}x^2+Z'_{½}x^3\right)\left(Z_{½}+Z_{½}x^2+Z_{½}x^3\right)+\left(Z'_3y^9+Z'_2y^{-3}+Z'_1y^{-11}-2Z'_{½}Z_{½}\right)}{x^{-6}\left(Z_{½}+Z_{½}x^2+Z_{½}x^3\right)^2+\left(Z_3y^9+Z_2y^{-3}+Z_1y^{-11}+y^{-15}-Z_{½}^2\right)} \tag{4}$$

where $h = \frac{g\mu_B}{k_B}B$, $Z_s(t) = \frac{\sinh(t[s+1/2])}{\sinh(t/2)}$ is the partition function of a single half-integer spin s as a function of the dimensionless magnetic field $t = \frac{h}{T}$, and its derivative is given by

$$Z'_s(t) = (s+1/2)\frac{\cosh(t[s+1/2])}{\sinh(t/2)} - \frac{\sinh(t[s+1/2])\cosh(t/2)}{2\sinh^2(t/2)}.$$

x and y are defined below Equation (3). The approximate result in Equation (4) can again be checked against the complete numerical solution yielding very good agreement for at least $|J'/J| \leq 0.1$ for all relevant temperatures.

The calculated magnetization curves for a model with nonuniform exchange couplings with J/k_B = –72.5 K and J'/k_B = –7 K (g = 2.10) are shown in Figure 6 as solid lines. As shown in Figure 6, we have obtained a very satisfactory agreement with the experimental data for the complex $[Cu_6\{(MeSiO_2)_6\}_2]\cdot 6DMF$ over the whole temperature range under investigation, except for data taken at T = 2 K. The deviations between theory and experiment become visible below 5 K. However, we should note once more that the magnetization curve at T = 2 K can be nicely simulated

by using a Brillouin function for isolated particles with S = 3 and g = 2.00 (dashed line) or by using our nonuniform exchange model with an effective g-value of 2.00 (short dashed line). We would like to point out however that the same conceptual problem arises in ref.[8]: The low-temperature magnetization of the complex $\{[Cu_6\{(PhSiO_2)_6\}_2]\cdot 5BuOH\}\cdot 3^nBuOH$ also shows a saturation value expected for S = 3 with g = 2.00.

ESR Measurements

In two papers reported only recently,[8,9] high-frequency ESR (HF-ESR) techniques were used to investigate polycrystalline powder samples of $[Cu_6\{(PhSiO_2)_6\}_2]\cdot 6EtOH$ and $\{[Cu_6\{(PhSiO_2)_6\}_2]\cdot 5BuOH\}\cdot 3^nBuOH$ to study the nature of the ground spin state of ferromagnetic rings and to obtain the effective magnetic anisotropy parameters of paramagnetic clusters. It was demonstrated that two sets of the equally spaced resonances at high exciting frequency might be attributed to the parallel and perpendicular transitions of an anisotropic paramagnet with an effective S = 3 spin and unresolved rhombicity (E = 0). The sign of the zero-field splitting parameter $D > 0$ corresponds to a hard-axis type anisotropy. The molecular g-tensor shows an axial symmetry with an unusual feature of "reversed" g-values ($g_\parallel < g_\perp$), which is not in accordance with the expected correlation ($g_\parallel > g_\perp$) for the local g-tensor with a square-pyramidal environment of the copper centres. Notably, there are still two small questions in the interpretation of magnetic data based on a uniform/nonuniform microscopical model, which the HF-ESR measurements on polycrystalline powder samples did not answer. (i) The reported magnetic anisotropy parameters D (0.3 and 0.308 cm^{-1}) are quite similar, showing that the initial splitting of the S = 3 manifold remains almost insensitive to the anisotropy of exchange interactions within the ring (uniform and nonuniform exchange cases). (ii) The absence of additional transitions to the variable-temperature HF-ESR polycrystalline spectra in the temperature range up to 100 K may indicate that the ground S = 3 state of a molecular cluster is well thermally isolated from the other excited multiplets.

Performing the resonance measurements on single crystals of $[Cu_6\{(MeSiO_2)_6\}_2]\cdot 6DMF$, a more complicated situation than that described in the literature was found. Single-crystal ESR spectra were recorded using the cavity technique in the frequency range 26–56 GHz with an opportunity of a sample rotation in three mutually perpendicular planes. The ESR spectra at 38.816 GHz (T = 1.5 K) for two different directions of the magnetic field are shown in parts a and b of Figure 7. Each spectrum consists of up to 20 well-resolved absorption lines (ESR active) with an average line width in the order of 28 mT. The angular dependence of the resonance line positions shows the strong magnetic anisotropy. The appearance of the spectrum with multicomponent structure may be interpreted as follows: (1) The energy spectrum of individual clusters is strongly anisotropic; consequently the presence of two nonequivalent molecules in the unit cell with an angle of 51.5° between the local axial axis might double the ESR spectrum (in the literature[8,9] this effect is not observed or discussed for polycrystalline powder samples). (2) According to a nonuniform model, the excited states (S = 2, 1, 0) of the molecular cluster of $[Cu_6\{(MeSiO_2)_6\}_2]\cdot 6DMF$ are close to each other and to the ground multiplet S = 3 (in the distance of a few Kelvins); all of the states are split, consequently the extra transitions between different sublevels inside and/or between different multiplets are possible.

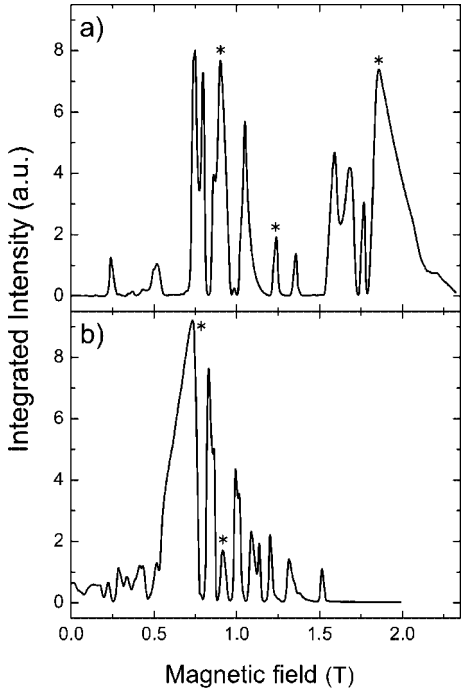

Figure 7. ESR spectra recorded on a single-crystal sample of $[Cu_6\{(MeSiO_2)_6\}_2]\cdot 6DMF$ at 38.816 GHz (T = 1.5 K). (a) Parallel and (b) perpendicular to the axial axis of a molecule.

In the case of a few close multiplets, the ESR spectra for a S = 3, 2 or 1 system can be interpreted separately for each manifold by the effective spin Hamiltonian

$$H = D[S_x^2 - 1/3S(S+1)] + E(S_x^2 - S_y^2) + \mu_B \mathbf{S}\cdot\mathbf{g}\mathbf{B},$$

in which each set of anisotropic parameters D, E, $\mathbf{g}$ will correspond to the given effective spin S = 3, 2 or 1. It should be stressed that D, E, $g_\parallel$, $g_\perp$ are effective parameters for an effective spin S, and they cannot be used directly in the microscopic model (1). A single ion anisotropy is not possible for a spin S = 1/2 (Cu^{2+} ions) and only an effective anisotropy term D of the complete molecule can arise from an anisotropy of the exchange interactions within the ring. The molecular g-tensor for a given geometry is related in a complicated way to the local g-tensors of individual Cu sites.

Analysis of the resonance data reveals that some lines of the spectrum (marked by * symbols in Figure 7) might be attributed to transitions for the split S = 3 multiplet with unresolved rhombicity, as reported for polycrystalline pow-

der measurements.[8,9] The magnetic anisotropic parameters obtained for the split $S = 3$ multiplet are: $g_{\parallel} = 2.05$, $g_{\perp} = 2.22$, $D = 14.5$ GHz (0.48 cm^{-1}) and $E = 0$. The value of the zero-field splitting parameter D is in good agreement with the estimation obtained from the single-crystal X-band spectra of $[Cu_6\{(MeSiO_2)_6\}_2]$·6DMF. Single-crystal ESR measurements have confirmed an unchangeable character of the molecular g-tensor with good accuracy for polymetallaorganosiloxane complexes. It should be noted that the larger magnitude of the effective anisotropy parameter D of the $S = 3$ manifold for the given complex indicates the larger anisotropy of exchange interactions within the ring compared to the previously reported analogues.[8,9]

A weak ferromagnetic intertrimer coupling $|J'/k_B| = 7$ K produces the total energy splitting of $4/3|J'/k_B| = 9.33$ K between idealized (non-split) $S = 3$ and $S = 0$ states (see energy-level scheme for the coupling of two "effective $S = 3/2$ spins" in Figure 5). Note, the energy interval to the nearest excited state $S = 2$ takes half of this value and is 4.67 K. For the obtained effective parameter $D = 14.5$ GHz the expected total splitting of the $S = 3$ state is 6.26 K. Thus, if we assume that all close states $S = 3, 2, 1$ are split by anisotropy of exchange interactions within the ring then the energy overlap or superposition of the different sublevels associated with the different manifolds is expected. According to this complication, a classification of all detected resonances in the frame of all possible transitions for excited and ground states was avoided. We consider that the other ESR-active lines, which are not marked in Figure 7, might be associated to the sublevel transitions for the split $S = 2$ and $S = 1$ states and their satellites arising from a second independent molecule. The slightly different values of the effective anisotropy parameter D for the $S = 2$ and $S = 1$ states compared with the corresponding value for the $S = 3$ state are expected.

Conclusions

This paper reports on the synthesis, X-ray crystal structure and magnetic properties of a new oxygen-bridged hexanuclear copper(II) hexamethylcyclohexasiloxane complex, $[Cu_6\{(MeSiO_2)_6\}_2]$·6DMF. In contrast to the known phenyl analogues, the present complex has methyl groups as substituents at the silicon atoms. This compound has a sandwich-like molecular structure. The molecule contains a planar ring of six oxygen-bridged Cu^{II} atoms arranged in an almost regular hexagon and sandwiched by two hexamethylcyclohexasiloxanolate ligands.

Investigations of the magnetic properties in the high-temperature region have shown that the molecular complex has a strong average ferromagnetic Cu–Cu exchange interaction of $|J_{av}/k_B| = (50.4 \pm 1)$ K, which produces a high-spin $S = 3$ molecular ground state. Yet, at temperatures below about 100 K, significant deviations between the experimental susceptibility data and the theory for a model with uniform nearest-neighbour exchange couplings become visible. Because of rather large intermolecular distances and the absence of an apparent exchange path, intermolecular interactions of either dipolar or exchange type do not seem likely. Attempts to modify the uniform-exchange model by including weakly anisotropic intramolecular exchange terms (because of slight distortions of copper–oxygen exchange bridges) or next-nearest neighbour exchange do not lead to a satisfactory agreement with the experimentally observed curve either. However, good fits for the magnetic susceptibility and the magnetization in the whole accessible temperature and field range can be obtained from an isotropic Heisenberg model that has nonuniform nearest-neighbour exchange couplings corresponding to weakly coupled trimers with a strong ferromagnetic intratrimer exchange coupling of $|J/k_B| = 72.5$ K and a weak ferromagnetic intertrimer exchange coupling of $|J'/k_B| = 7$ K.

Such dramatic variations in the magnitude of the exchange couplings within the ring might seem surprising in light of the almost regular hexagonal arrangement of the Cu^{2+} ions. However, it is well known that small variations in the bonding angles of oxygen exchange bridges can significantly influence the exchange couplings. For the family of the ring-shaped polynuclear Cu^{II} cyclomethylsiloxanolate complexes, the critical bonding angle of the oxygen bridge Cu–O–Cu for a transition between ferromagnetic and antiferromagnetic exchange is approximately 96°.[10] Yet, it seems plausible that the highest bonding angles of about 94° (see Table 1) might be close enough to the critical angle that the corresponding exchange coupling is significantly reduced compared to the other two. Our results thus seem to suggest that the magnetic properties of quantum rings are very susceptible to small structural infringements of symmetry, which at once effectively split the ring as a whole into a system with simpler blocks: poorly cooperating trimers or dimers.

Experimental Section

General Remarks: All chemicals used were of high quality and purchased from Aldrich. The solvents were dried and distilled prior before use. Calculations on KOH were made based on the content of KOH (85%, Aldrich).

Synthesis of $[Cu_6\{(MeSiO_2)_6\}_2]$·6DMF: $MeSi(OEt)_3$ (10 mL, 0.05 mol), KOH (3.3 g, 0.05 mol), water (0.9 mL, 0.05 mol) and MeOH (80 mL) were added to toluene (80 mL) under vigorous stirring. The reaction mixture was stirred for 45 min at room temperature and then heated up to the boiling point. A solution of $CuCl_2$ (3.4 g, 0.025 mol) in MeOH (80 mL) was added dropwise. The reaction mass was refluxed for 10 min and filtered. The solution was evaporated and dried in vacuo (1 Torr, at 80 °C). A greenish-blue crystalline product **D** (see Scheme 1) was obtained. Yield: 4.43 g (82.5%). This product was dissolved in DMF (50 mL) under heating and left to crystallize. The recrystallization process took a few months and transparent greenish-blue crystals, suitable for the X-ray structure analysis, were obtained. $C_{30}H_{78}Cu_6N_6O_{30}Si_{12}$ (1721.30): C 20.93, H 4.57, N 4.88; found C 20.19, H 4.53, N 4.58.

Trimethylsilylation of Product D: A mixture of product **D** (1.5 g, 1.2 mmol) and pyridine (3.5 mL, 43.2 mmol) was slowly stirred for 15 min. Me_3SiCl (7.28 mL, 7.6 mmol) was added while slowly stirring. The reaction mixture was stirred for another 10 min at room

temperature and then hexane (30 mL) was added. The solution was heated and refluxed for 55 min. The mixture was cooled to room temperature, washed with water to remove Cl^-, dried with Na_2SO_4 and the solvent was evaporated. A viscous colourless product was obtained after drying in vacuo (1 Torr, at 50 °C, 1 h). Yield: 0.56 g (53.57%). ^{1}H NMR: δ = 0.11 (s, 9 H, –OSiMe$_3$), 0.03 (s, 3 H, MeSiO$_3$–) ppm. ^{29}Si NMR: δ = 8.50 (s, –OSiMe$_3$), –68.18 (s, MeSiO$_3$–) ppm.

Single-Crystal X-ray Crystallography: A single crystal (greenish-blue block with dimensions $0.52 \times 0.49 \times 0.37$ mm) was measured on a Stoe-IPDS-II diffractometer in ω-scan mode. An empirical absorption correction was performed using the MULABS option[17] in PLATON.[18] Structure solution was performed by direct methods using SHELXS-97[19] and structure refinement by full-matrix least-squares on F^2 with SHELXL-97.[20] Hydrogen atoms were placed at ideal positions and refined with fixed isotropic displacement parameters using a riding model.

Detailed crystal data and experimental parameters are given in Table 2.

Table 2. Crystal data and structure refinement for [Cu$_6${(MeSiO$_2$)$_6$}$_2$]·6DMF.

Empirical formula	$C_{30}H_{78}Cu_6N_6O_{30}Si_{12}$
Crystal dimensions [mm]	$0.52 \times 0.49 \times 0.37$
F_w [g/mol]	1721.30
T [K]	173(2)
λ [Å]	0.71073
Crystal system, space group	monoclinic, $P2_1/n$
a [Å]	13.3728(5)
b [Å]	15.4281(7)
c [Å]	17.4335(7)
β [°]	98.932(3)
V [Å^3]	3553.2(3)
Z	2
Absorption coefficient [mm^{-1}]	2.048
F(000)	1764
ρ_{calcd} [g/cm^3]	1.609
θ range for data collection [°]	2.64–30.55
Reflections collected/unique	64952/10746 [R_{int} = 0.0494]
Completeness to θ = 30.55 [%]	98.7
Absorption correction	semiempirical
Max. and min. transmission	0.5187 and 0.4164
Data/restraints/parameters	10746/0/385
Goodness-of-fit	0.938
R_1, wR_2 [$I > 2\sigma(I)$]	0.0257, 0.0659
R_1, wR_2 [all data]	0.0334, 0.0678
Max./min. peak [e/Å^3]	0.381, –0.960

CCDC-630857 contains the supplementary crystallographic data for this paper. These data can be obtained free of charge from The Cambridge Crystallographic Data Centre via www.ccdc.cam.ac.uk/data_request/cif.

Magnetic Susceptibility and Magnetization Measurements: Variable-temperature magnetic susceptibility measurements in the temperature range 2–350 K and magnetic fields 0.01–0.2 T were carried out on a polycrystalline sample (m = 97.85 mg) using a Quantum Design SQUID magnetometer MPMS-XL. These measurements were complemented by isothermal magnetization runs at temperatures between 2 and 200 K for fields up to 5 T.

NMR Measurements: ^{1}H and ^{29}Si NMR spectra were recorded with a Bruker Avance 400 spectrometer (^{1}H, 400.13 MHz; ^{29}Si, 79.495 MHz) at 30 °C in $CDCl_3$. Chemical shifts (δ, ppm) were measured relative to TMS (δ = 0.00 ppm).

ESR Measurements: Powder and single-crystal ESR spectra of the compound [Cu$_6${(MeSiO$_2$)$_6$}$_2$]·6DMF were recorded employing various spectrometers operating on different fixed frequencies in the range 9.5–134 GHz equipped with a variable-temperature Oxford cryostat with an accessible temperature range of 1.4–300 K.

Supporting Information (see also footnote on the first page of this article): View of the crystals (Figure S1), comparison of the magnetic susceptibility data with calculations for alternative models (Figures S2, S3 and S4) and the calculated magnetization curves for uniform and nonuniform models (Figure S5).

Acknowledgments

The work was supported by the Deutsche Forschungsgemeinschaft (DFG) (Forschergruppenprogramm "Spin- und Ladungskorrelationen in niedrigdimensionalen metallorganischen Festkörpern", FOR412). We thank J. Bats (Institut für Anorganische Chemie, J. W. Goethe-Universität Frankfurt) for the collection of the X-ray data.

[1] D. Gatteschi, A. Caneschi, L. Pardi, R. Sessoli, *Science* **1994**, *265*, 1054–1058.
[2] S. P. Watton, P. Fuhrmann, L. E. Pence, A. Caneschi, A. Cornia, G. L. Abbati, S. J. Lippard, *Angew. Chem. Int. Ed. Engl.* **1997**, *36*, 2774–2776.
[3] V. Pashchenko, B. Brendal, B. Wolf, M. Lang, K. Lyssenko, O. Shchegolikhina, Yu. Molodtsova, L. Zherlitsyna, N. Auner, F. Schütz, M. Kollar, P. Kopietz, N. Harrison, *Eur. J. Inorg. Chem.* **2005**, *22*, 4617–4625.
[4] V. A. Igonin, O. I. Shchegolikhina, S. V. Lindeman, M. M. Levitsky, Yu. T. Struchkov, A. A. Zhadnov, *J. Organomet. Chem.* **1992**, *423*, 351–360.
[5] C. Zucchi, O. I. Shchegolikhina, M. Borsari, A. Cornia, G. Gavioli, A. C. Fabretti, E. Rentschler, D. Gatteschi, R. Ugo, R. Psaro, Yu. A. Pozdniakova, S. V. Lindeman, A. A. Zhdanov, G. Pályi, *J. Mol. Catal. A* **1996**, *107*, 313–321, and references therein.
[6] S. V. Lindeman, O. I. Shchegolikhina, Yu. A. Molodtsova, A. A. Zhdanov, *Acta Crystallogr., Sect. C: Cryst. Struct. Commun.* **1997**, *53*, 305–309.
[7] Yu. T. Struchkov, S. V. Lindeman, *J. Organomet. Chem.* **1995**, *488*, 9–14.
[8] G. L. Abbati, A.-L. Barra, A. Caneschi, A. Cornia, A. F. Costantino, D. Gatteschi, Yu. A. Pozdniakova, O. I. Shchegolikhina, *C. R. Chim.* **2003**, *6*, 645–656.
[9] E. Rentschler, D. Gatteschi, A. Cornia, A. C. Fabretti, A.-L. Barra, O. Shchegolikhina, A. A. Zhdanov, *Inorg. Chem.* **1996**, *35*, 4427–4431.
[10] V. Pashchenko, M. Lang, B. Wolf, L. Zherlitsyna, N. Auner, O. Shchegolikhina, Yu. Pozdnyakova, F. Schütz, P. Kopietz, M. Kollar, *C. R. Chim.* **2007**, *10*, 89–95.
[11] Yu. A. Pozdniakova, M. Antipin, O. I. Shchegolikhina, D. Katsoulis, N. Auner, B. Herrschaft, *Organometallics* **2000**, *19*, 1077–1082.
[12] O. I. Shchegolikhina, I. V. Blagodatskikh, A. A. Zhdanov in *Tailor-Made Silicon-Oxygen Compounds. From Molecules to Materials* (Eds.: R. Corriu, P. Jutzi), Vieweg, Wiesbaden, Germany, **1996**, p. 177.
[13] Yu. A. Molodtsova, Yu. A. Pozdniakova, K. A. Lyssenko, I. V. Blagodatskikh, D. E. Katsoulis, O. I. Shchegolikhina, *J. Organomet. Chem.* **1998**, *571*, 31–36.
[14] a) E. König, *Magnetic Properties of Coordination and Organo-Metallic Transition Metal Compounds*, in Landolt-Börnstein, Neue Serie, Springer, Berlin, **1966**, vol. II/2, pp. 1–16; b) R. Boča, *Theoretical Foundations of Molecular Magnetism*, vol. 1, *Current Methods in Inorganic Chemistry*, Elsevier, Amsterdam, **1999**, appendix 4.

[15] D. C. Johnston, R. K. Kremer, M. Troyer, X. Wang, A. Klümper, S. L. Bud'ko, A. F. Panchula, P. C. Canfield, *Phys. Rev. B: Condens. Matter* **2000**, *61*, 9558–9606 and references cited therein.
[16] D. Kouzoudis, *J. Magn. Magn. Mater.* **1998**, *189*, 366–376; D. Kouzoudis, *J. Magn. Magn. Mater.* **1997**, *173*, 259–265.
[17] R. H. Blessing, *Acta Crystallogr., Sect. A: Found. Crystallogr.* **1995**, *51*, 33–38.
[18] A. L. Spek, *J. Appl. Crystallogr.* **2003**, *36*, 7–13.
[19] G. M. Sheldrick, *Acta Crystallogr., Sect. A: Found. Crystallogr.* **1990**, *46*, 467–473.
[20] G. M. Sheldrick, *SHELXL-97, A Program for the Refinement of Crystal Structures*, University of Göttingen, Germany, **1997**.
Received: December 15, 2006
Published Online: August 28, 2007

